Aerosol and Air Quality Research

ORIGINAL RESEARCH
https://doi.org/10.4209/aaqr.2020.07.0455

Chemical Looping Combustion of Isopropanol in Aqueous Solution with Fabricated Fe_2O_3/Al_2O_3 and $Fe_2O_3/Al_2O_3/TiO_2$ Oxygen Carriers

Hsuan-Chih Wu, Young Ku*

Department of Chemical Engineering, National Taiwan University of Science and Technology, Taipei 106, Taiwan

ABSTRACT

Iron-based oxygen carriers supported on alumina or alumina/titania were fabricated and evaluated for chemical looping combustion of isopropanol (IPA). Hydrogen is the major combustible gas generated by IPA decomposition prior to combustion with oxygen carriers at temperatures above 800°C. Nearly complete combustion (above 95%) of IPA was achieved for experiments conducted with fabricated Fe_2O_3/Al_2O_3 and $Fe_2O_3/Al_2O_3/TiO_2$ operated at lower inlet IPA flow rates. Carbon deposition during the chemical looping combustion of IPA was minimized using $Fe_2O_3/Al_2O_3/TiO_2$ as an oxygen carrier. The reduction of Fe_2O_3/Al_2O_3 and $Fe_2O_3/Al_2O_3/TiO_2$ by hydrogen was markedly increased with increasing inlet hydrogen concentration (5–20%), and was not obviously influenced by operating temperature (875–925°C). According to the shrinking core model, the mass transfer coefficients (k_g) of Fe_2O_3/Al_2O_3 and $Fe_2O_3/Al_2O_3/TiO_2$ reduction with H_2 were found to be 0.22 and 0.24 mm s^{-1}, while the effective diffusion diffusivity (D_e) of Fe_2O_3/Al_2O_3 oxygen carriers was more easily depended on the oxygen carrier conversion. The higher reduction conversions obtained for experiments conducted with $Fe_2O_3/Al_2O_3/TiO_2$ because it can be further reduced to FeO and Fe; comparing to those with Fe_2O_3/Al_2O_3, which is primarily reduced to FeO. Hydrogen molecules are found to diffuse more easily through the FeO product-layer on Fe_2O_3/Al_2O_3 than the FeO/Fe product-layer on $Fe_2O_3/Al_2O_3/TiO_2$.

Keywords: Chemical looping, Isopropanol, Reaction kinetics, Hydrogen, Fe_2O_3, Al_2O_3, Fabricated, Moving bed reactor

Received: July 28, 2020
Revised: October 12, 2020
Accepted: October 16, 2020

* **Corresponding Author:**
ku508@mail.ntust.edu.tw

Publisher:
Taiwan Association for Aerosol Research
ISSN: 1680-8584 print
ISSN: 2071-1409 online

1 INTRODUCTION

Liquid waste combustion by chemical looping technology is aimed to eliminate liquid waste and simultaneously to generate hydrogen and/or heat. For chemical looping combustion (CLC) operation, the metal oxides provided the lattice oxygen to react with the fuel. Subsequently, the reduced particles are oxidized by air for cyclic applications. However, liquid injection is a critical concern for CLC operation, and is greatly influenced by the characteristics of liquid feedstocks. The mode of liquid fuel injection for CLC operation includes direct injection into the combustor, reforming before injection, and vaporization before injection. Because the temperature for the thermal pyrolysis of fuel is usually lower than that for fuel vaporization, fuel reforming to generate combustible gases for combustion with oxygen carriers would be preferred. Satisfactory hydrogen production for chemical looping reforming (CLR) of waste lubricating oil, waste cooking oil, scrap tyre pyrolysis oil (STPO) and other liquid fuels with NiO/Al_2O_3 oxygen carriers were reported by various researchers (Lea-Langton *et al.*, 2010; Pimenidou *et al.*, 2010; Giannakeas *et al.*, 2012). However, the deterioration of hydrogen production was observed after multi-cycle operations, possibly due to the fouling of oxygen carriers by the carbon deposition or poisoning by the trace additives in the fuels. However, Serrano *et al.* (2017) investigated the application of Fe_2O_3/Al_2O_3 for chemical looping of combustion diesel and lubricant oil, and reported that the reactivity of Fe_2O_3/Al_2O_3 oxygen carriers was not affected by sulphur or impurities present in the

fuels. This is because the formation of iron sulfide is thermodynamically feasible only under sub-stoichiometric conditions (fuel-rich), so sulphur does not react with the components existing in the Fe-based oxygen carrier during the combustion process.

Isopropanol (IPA) is a widely used solvent in semiconductor and liquid crystal display (LCD) industries for cleansing wafers and panels in the fabrication process (Ku *et al.*, 2007). Spent solvents of high IPA concentrations, usually 30 wt.% or higher, may be considered to recover IPA. However, further treatment of spent solvents of lower IPA concentrations may be a serious concern for these industries. Chiu *et al.* (2014a) studied the IPA combustion with Fe_2O_3/Al_2O_3 in a moving-bed reactor, indicating that the IPA conversion and CO_2 yield of IPA combustion reached nearly 100% for experiments conducted at 900°C. The result also indicated that the processing efficiency was declined dramatically for lower IPA content, and when the IPA content is lower than 10%, the processing efficiency would be negative. The heat is possibly insufficient as process heat loss is included in a realistic CLC system for a very dilute solution as fuel in CLC. Hence, the IPA solution containing 10 vol.% IPA was selected to be the target liquid fuel. In this study, alumina- and alumina/titania-supported Fe_2O_3 (Fe_2O_3/Al_2O_3 and $Fe_2O_3/Al_2O_3/TiO_2$) were fabricated to employ as oxygen carriers for the chemical looping combustion of aqueous solution containing 10 vol.% IPA. The reduction kinetics of the fabricated oxygen carriers with hydrogen was examined and described by a shrinking core model (SCM).

2 MATERIAL AND METHODS

2.1 Preparation of Various Iron-based Oxygen Carriers

In this study, Fe_2O_3/Al_2O_3 oxygen carriers were formulated with 60 wt.% hematite (99.9% Fe_2O_3, China Steel) and 40 wt.% alumina (99% Al_2O_3, Chin Jung). $Fe_2O_3/Al_2O_3/TiO_2$ were formulated with 70 wt.% hematite, 20 wt.% alumina and 10 wt.% titania. Predetermined amounts of hematite, alumina and titania particles of roughly 1 μm were mixed thoroughly in deionized water at room temperature. The well-mixed slurry was desiccated at 130°C for 10 hours, and was subsequently crushed and partitioned for particles of size between 1.2 and 1.4 mm. The Fe_2O_3/Al_2O_3 and $Fe_2O_3/Al_2O_3/TiO_2$ particles were later sintered in a muffle furnace for 2 hours.

The crush strength of fabricated Fe_2O_3/Al_2O_3 and $Fe_2O_3/Al_2O_3/TiO_2$ was respectively determined to be 30.53 and 10.25 N by a texture machine (TA.XT plus). The attrition of fabricated Fe_2O_3/Al_2O_3 and $Fe_2O_3/Al_2O_3/TiO_2$ was correspondingly determined to be 4.01 and 16.83% by an attrition analyzer following ASTM methods D4058-96. The particle density and porosity of oxygen carriers were measured by the Archimedes method in water. The particle densities of fabricated Fe_2O_3/Al_2O_3 and $Fe_2O_3/Al_2O_3/TiO_2$ were determined to be 2,377 kg m^{-3} and 1,937 kg m^{-3}, while the porosity of 49.13% and 59.60% were measured for fabricated Fe_2O_3/Al_2O_3 and $Fe_2O_3/Al_2O_3/TiO_2$, respectively. The physical properties of these fabricated iron-based oxygen carriers are presented in Table 1.

2.2 Establishment of the Fixed-bed Reactor System

The fixed-bed reactor system employed in this study is composed of a stainless-steel tubular reactor and a PID-controlled heating element, as shown in Fig. 1. A plate with sixteen apertures of 0.25 mm in diameter was located in the lower segment of the reactor for supporting fabricated oxygen carriers. The temperature of the loaded reactor was then raised and eventually maintained at designated operating temperature. Hydrogen/nitrogen gas mixture was introduced into the reactor to reduce fabricated oxygen carriers. The outlet gas from the reactor was passed through

Table 1. Physical properties determined for the fabricated iron-based oxygen carriers.

Parameters	Unit	Fe_2O_3/Al_2O_3	$Fe_2O_3/Al_2O_3/TiO_2$
Fe_2O_3 fraction	wt.%	60	70
Particle size	mm	1.2–1.4	1.2–1.4
Particle density, ρ_p	kg m^{-3}	2377	1937
Porosity	%	49.13	59.60
Crushing strength	N	30.53	10.25
Attrition	%	4.01	16.83

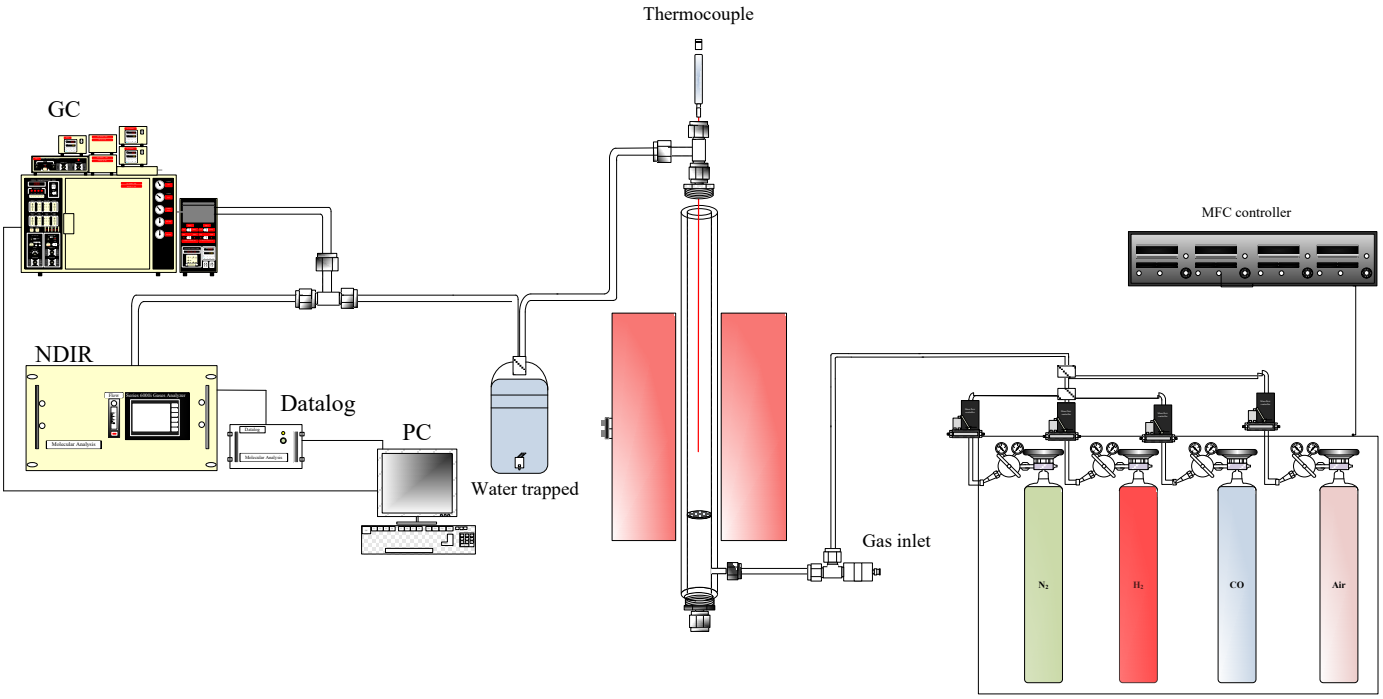

Fig. 1. Schematic diagram of the fixed-bed reactor system for CLP operation.

a cold trap to condense steam, and was consequently analyzed by a non-dispersive infrared sensor (NDIR, Molecular Analysis 6000i) and a gas chromatography equipped with a thermal conductivity detector (GC-TCD, China Chromatography 2000) to detect the concentrations of carbon dioxide, carbon monoxide, methane, hydrogen, and oxygen. After reduction, nitrogen was introduced for sweeping residual gas contained in the reactor. Air at flowrate of 1 L min^{-1} was subsequently introduced for 30 minutes to oxidize the reduced oxygen carriers for further replicate operations.

2.3 Establishment of the Moving-bed Reactor System

Schematic diagram of the annular dual-tube moving-bed reactor system (ADMBR) employed in this study is shown in Fig. 2. The reactor system was composed of a stainless-steel dual-tubular reactor and with a PID-controlled heating element, and two screw conveyors. For empty-bed operations of the ADMBR, the temperature for experiments was maintained at 850, 875, or 900°C. Aqueous solution containing 10% IPA was introduced into the inner tube with nitrogen. The gaseous products generated by thermal decomposition of IPA were then flown through the inner tube into the spacing between inner and outer tubes.

For moving-bed operations, the fabricated oxygen carriers were initially packed in the spacing between inner and outer tubes of the ADMBR before operation. Supplementary oxygen carriers were then continuously fed into the packed reactor by a screw conveyer after the reactor was heated up to predetermined temperatures. For iron-based oxygen carrier, the fuel reactor should be operated above 750°C to avoid carbon deposition from methane decomposition (Zeng *et al.*, 2015). However, the iron-based oxygen carrier at an operating temperature above 1200°C may form fusion and sintering, which can cause solid flow and particle reactivity problems. Hence, the operating temperature of the chemical looping system is typically in the range from 750 to 1200°C, according to previous studies (Fan *et al.*, 2015). In this study, the temperature of the ADMBR was operated to about 900°C is due to the limitation of the heating element. IPA solution carried by nitrogen was then introduced into the inner tube for consequent combustion with fabricated oxygen carriers. The reduced oxygen carriers were collectively removed out of the reactor by another screw conveyor. The outlet gas from the reactor was cooled by a cold trap to condense water vapor and was analyzed by a GC-TCD and by a NDIR to detect H_2, CO_2, CO, CH_4, and O_2. The phase characteristics of fresh, reduced and regenerated oxygen carriers were detected by X-ray diffraction (XRD).

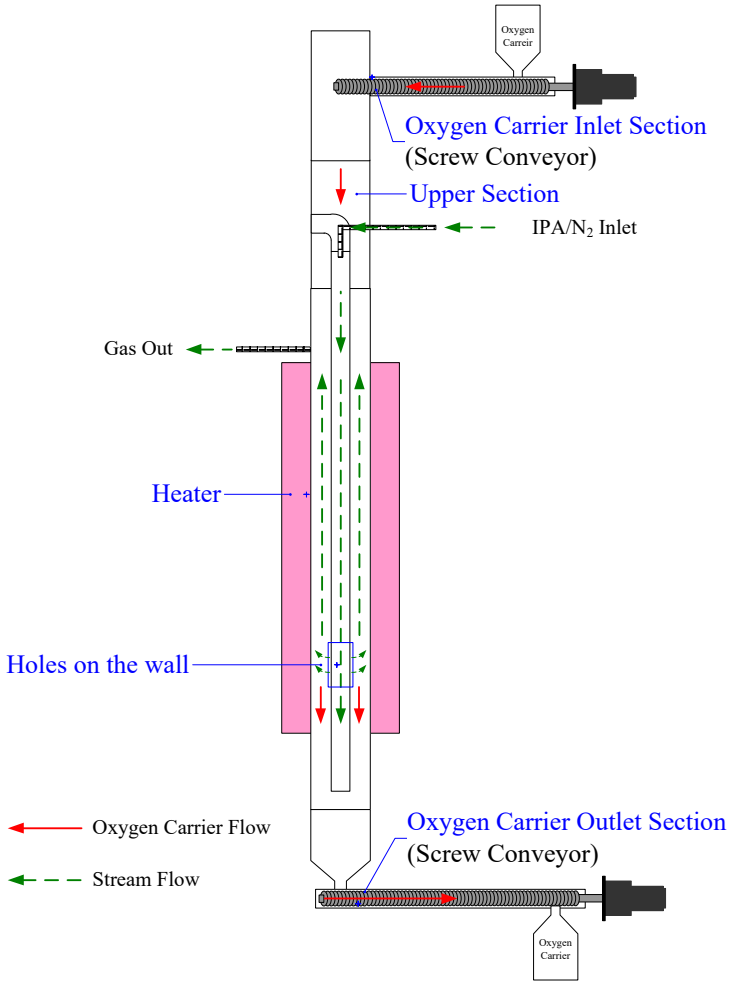

Fig. 2. Schematic diagram of the annular dual-tube moving-bed reactor (ADMBR) employed in this study.

3 RESULTS AND DISCUSSION

3.1 Decomposition of IPA in the Empty-bed Reactor

Effect of operating temperature on the fuel gas composition on IPA solution decomposition was investigated in an empty-bed reactor. As illustrated in Fig. 3, experimental results suggest that nearly complete IPA decomposition could be accomplished, and the main components of cooled outlet streams were determined to be H_2, CO_2, CH_4 and CO. IPA is assumed to be decomposed to form CH_4 and CO, which are subsequently reacted with H_2O to carry out the methane reforming and water-gas shift reactions, respectively. The reactions involved are described as:

$$C_3H_7OH \longrightarrow 2CH_4 + CO \quad (1)$$

$$CH_4 + H_2O \longrightarrow CO + 3H_2 \quad (2)$$

$$CO + H_2O \longrightarrow CO_2 + H_2 \quad (3)$$

However, the exothermic water-gas shift reaction is not favorable for experiments conducted at higher operating temperatures, comparing to the endothermic methane reforming reaction. Thus, CH_4 and CO_2 concentrations were decreased, whereas H_2 and CO concentrations were slightly increased, with increasing operating temperature, comparable to the results reported by previous study (Chiu *et al.*, 2014a).

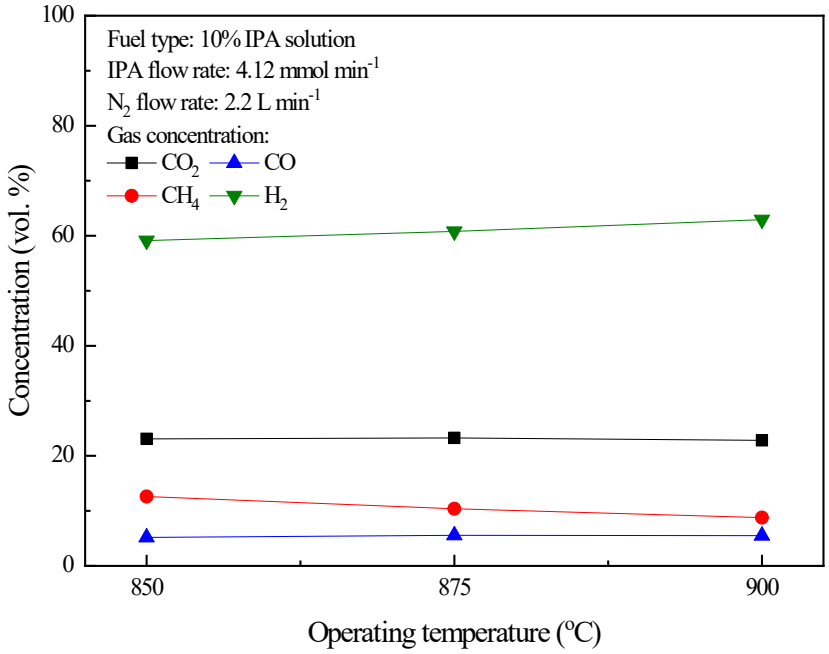

Fig. 3. Effect of operating temperature on the composition of cooled outlet stream for IPA combustion in the empty bed.

3.2 IPA Combustion with Fabricated Fe_2O_3/Al_2O_3 Oxygen Carriers in the ADMBR

Chemical looping combustion of IPA with fabricated Fe_2O_3/Al_2O_3 was conducted in the ADMBR operated at 900°C. The outlet gas was cooled to condense water vapor before further gas analysis. The main components of outlet streams for experiments operated with different inlet IPA flow rates were determined to be CO_2, CH_4, H_2 and CO, as shown in Fig. 4. Outlet gas containing nearly 100% CO_2 was achieved for experiments conducted with inlet IPA flow rate of 4.1 mmol min^{-1}. However, CO_2 concentration of outlet gas was found to be decreased, while CH_4 concentration was increased, for experiments carried out with higher inlet IPA flow rates, indicating that methane generated by IPA decomposition was not completely combusted by fabricated Fe_2O_3/Al_2O_3. Moreover, CO concentration of the outlet gas was slightly enhanced for experiments conducted with IPA flow rate ranged from 7.2 to 10.1 mmol min^{-1}, while H_2 concentration was notably increased.

The carbon deposition for experiments carried out with higher IPA flow rate were observed which may be ascribed to the cracking of methane generated by IPA decomposition was further decomposed to form carbon and hydrogen, as depicted by Reaction (4) (Cho *et al.*, 2005; Ku *et al.*, 2014).

$$CH_4 \longrightarrow C + 2H_2 \quad (4)$$

Based on carbon and hydrogen balance calculation, the steam generation rate (F_{Steam}) and carbon deposition rate (F_C) for IPA combustion are determined by Eqs. (5) and (6):

$$F_{Steam} = (4F_{IPA,in} + F_{H_2O,in}) - (2F_{CH_4} + F_{H_2}) \quad (5)$$

$$F_C = 3F_{IPA,in} - (F_{CH_4} + F_{CO_2} + F_{CO}) \quad (6)$$

where $F_{IPA,in}$ and $F_{H_2O,in}$ are the inlet mole flow rate (mmole min^{-1}) of IPA and H_2O, respectively; F_i is the outlet molar flow rate (mmole min^{-1}) of species i, i is denoted as CO_2, CO, H_2O, H_2 and CH_4. As shown in Fig. 4, the carbon deposition rate and steam generation rate of IPA combustion by fabricated Fe_2O_3/Al_2O_3 in the ADMBR were found to be increased for experiments conducted with higher IPA flow rates.

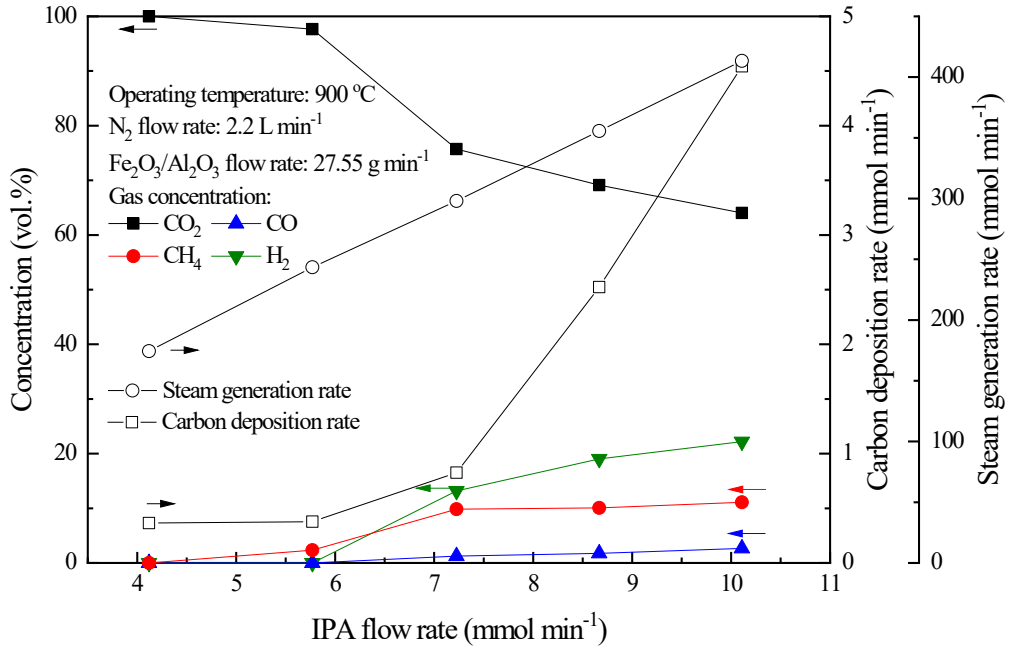

Fig. 4. Effect of IPA flow rate on the composition of cooled outlet stream for IPA combustion with Fe_2O_3/Al_2O_3 in the ADMBR.

The carbon conversion (X_C) is defined as the conversion of inlet IPA to carbonaceous gases (CO_2, CO and CH_4), as described as Eq. (7). IPA conversion (X_{IPA}) and oxygen carrier conversion (X_{OC}) for IPA combustion were determined by Eqs. (8) and (9) (Zeng *et al.*, 2015; Wu and Ku, 2016). The detailed mass balance data of the IPA combustion experiment, such as oxygen, carbon, hydrogen, and iron, were listed in Table 2.

$$X_C = \frac{F_{CO_2} + F_{CO} + F_{H_2O}}{3F_{IPA,in}} \tag{7}$$

$$X_{IPA} = \frac{\left(2F_{CO_2} + F_{CO} + F_{Steam}\right) - \left(F_{IPA,in} + F_{H_2O,in}\right)}{9F_{IPA,in}} \tag{8}$$

$$X_{OC} = \frac{\left(2F_{CO_2} + F_{CO} + F_{Steam}\right) - \left(F_{IPA,in} + F_{H_2O,in}\right)}{\left(\frac{x_{Fe_2O_3} \cdot \dot{m}_{OC}}{M_{Fe_2O_3}}\right) \times 1000 \times 3} \tag{9}$$

where $\dot{m}_{OC}$ is the mass flow rate (g min^{-1}) of the oxygen carriers.

As illustrated in Fig. 5, X_C and X_{IPA} are significantly decreased for experiments carried out with increasing inlet IPA flow rate, while less than 20% of the oxygen carrier conversion was achieved for most experiments, demonstrating the fabricated Fe_2O_3/Al_2O_3 was reduced mostly to Fe_3O_4, similar to the results reported by previous study (Luo *et al.*, 2014).

Based on the XRD patterns illustrated in Fig. 6, the main crystalline phases of reduced Fe_2O_3/Al_2O_3 for IPA combustion operated in the ADMBR, and the crystalline phases of reduced Fe_2O_3/Al_2O_3 were mostly Fe_3O_4 and Al_2FeO_4. Comparable observation was reported by previous researchers (Ishida *et al.*, 2005; Ku *et al.*, 2014). Zhu *et al.* (2016) analyzed the structural evolution during the reduction of α-Fe_2O_3 nanowires, and noticed that more oxygen vacancies were formed as the reduction continues. Thus, the rhombohedral-structured α-Fe_2O_3 was transformed to the cubic-structured Fe_3O_4. In this study, Fe_3O_4 was further reduced to form Al_2FeO_4. Al_2FeO_4 generated might serve as support materials as well as oxygen carriers in a moving-bed reactor for practical chemical looping operation, as stated by previous study (Chiu *et al.*, 2014b). Subsequently, the

Table 2. Summary of mass balance data for the IPA combustion experiment.

Inlet flow rate (mmol min^{-1})			Outlet flow rate (mmol min^{-1})								X_{OC}	X_C	X_{fuel}
IPA	H_2O	Fe_2O_3	H_2	CO	CO_2	CH_4	C	H_2O	Fe in OC	O in OC	%	%	%
IPA combustion with Fe_2O_3/Al_2O_3													
4.12	157.90	103.51	0	0	11.99	0.00	0.36	174.38	207.02	274.19	11.70	97.05	98.03
5.77	221.16	103.51	0	0	16.54	0.40	0.38	243.45	207.02	260.95	15.97	97.82	95.49
7.23	276.95	103.51	3.15	0.30	18.19	2.36	0.83	297.99	207.02	260.03	16.26	96.19	77.67
8.67	332.24	103.51	5.49	0.50	20.07	2.91	2.52	355.60	207.02	255.20	17.82	90.30	70.94
10.11	387.53	103.51	7.32	0.88	21.25	3.66	4.54	413.32	207.02	251.48	19.02	85.02	64.90
IPA combustion with $Fe_2O_3/Al_2O_3/TiO_2$													
4.12	157.90	119.38	0	0	11.87	0.24	0.25	173.90	238.76	322.52	9.95	97.99	96.07
5.77	221.16	119.38	0.01	0	16.90	0.25	0.16	243.72	238.76	307.54	14.13	99.10	97.43
7.23	276.95	119.38	0.01	0	21.05	0.58	0.05	304.68	238.76	295.53	17.48	99.75	96.27
8.67	332.24	119.38	1.19	0.25	21.97	3.04	0.74	359.63	238.76	295.23	17.57	97.15	80.64
10.11	387.53	119.38	0.03	0.00	23.58	3.38	3.37	421.19	238.76	287.42	19.74	88.88	77.71

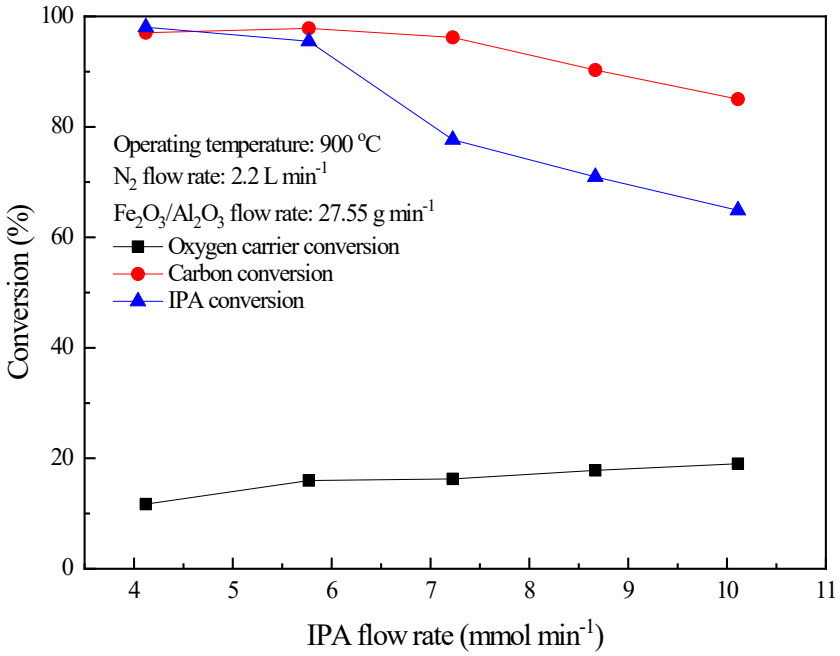

Fig. 5. Effect of IPA flow rate on fuel and oxygen carrier conversions for IPA combustion with Fe_2O_3/Al_2O_3 in the ADMBR.

reduced oxygen carriers were completely oxidized to Fe_2O_3 and Al_2O_3, which were observed in the XRD pattern.

3.3 IPA Combustion with Fabricated $Fe_2O_3/Al_2O_3/TiO_2$ in the ADMBR

Chemical looping combustion of IPA by fabricated $Fe_2O_3/Al_2O_3/TiO_2$ in the ADMBR was examined in this study. The composition of cooled outlet streams for combustion experiments of IPA was illustrated in Fig. 7. Outlet gas containing more than 97% CO_2 were achieved for experiments conducted with inlet IPA flow rate lower than 7.2 mmol min^{-1}, while the CO_2 concentration of outlet gas was dropped for experiments carried out with higher IPA flow rates. More CH_4, H_2 and CO were observed in the outlet gas for experiment conducted with IPA flow rate greater than 8.7 mmol min^{-1}, possibly because part of the combustible gas generated via Reactions (1) to (3) was not consumed by $Fe_2O_3/Al_2O_3/TiO_2$. However, CO_2 and CH_4 concentration of the outlet gas were found to be increased for experiment carried out with inlet IPA flow rate of 10.1 mmol min^{-1} than that with inlet IPA flow rate of 8.7 mmol min^{-1}, whereas H_2 and CO

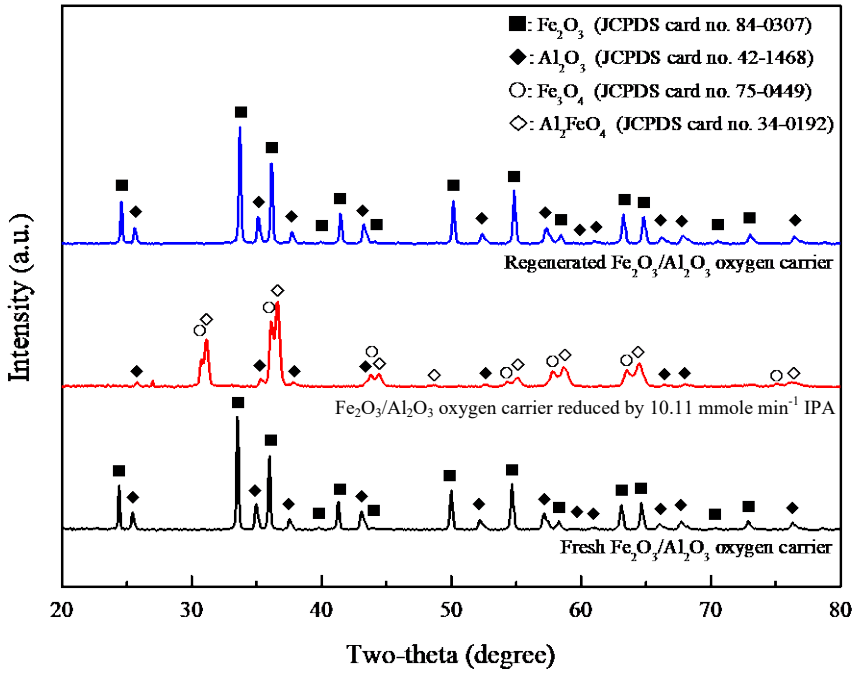

Fig. 6. X-ray diffraction patterns of fresh, reduced and regenerated Fe_2O_3/Al_2O_3 for IPA combustion.

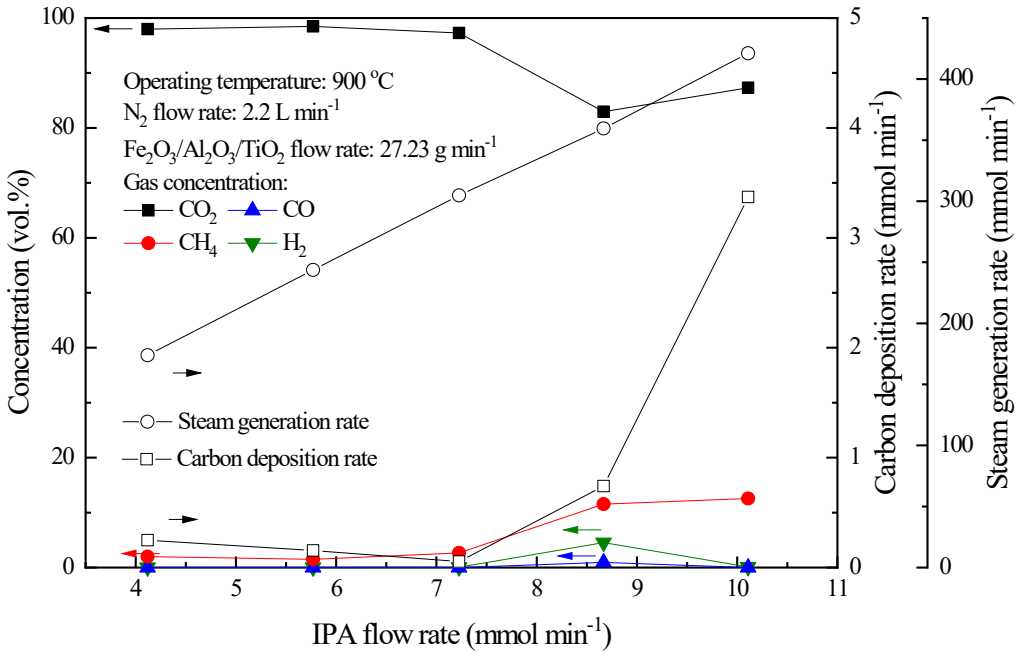

Fig. 7. Effect of IPA flow rate on the composition of cooled outlet stream for combustion of IPA with $Fe_2O_3/Al_2O_3/TiO_2$ in the ADMBR.

concentrations were decreased. Compared with the results by Fe_2O_3/Al_2O_3, more IPA was oxidized by $Fe_2O_3/Al_2O_3/TiO_2$ to generate more CO_2 and H_2O with less H_2 and CO. The calculated steam generation rates for IPA combustion with $Fe_2O_3/Al_2O_3/TiO_2$ were higher than those with Fe_2O_3/Al_2O_3, as demonstrated in Fig. 7.

As shown in Figs. 4 and 7, less carbon deposition were observed for IPA combustion with $Fe_2O_3/Al_2O_3/TiO_2$ than that with Fe_2O_3/Al_2O_3. CH_4 concentration of outlet gas was maintained at around 10% for IPA combustion with Fe_2O_3/Al_2O_3 and $Fe_2O_3/Al_2O_3/TiO_2$ with higher IPA flow rate. Fig. 8 demonstrates that carbon conversion, IPA conversion and oxygen carrier conversion for

experiments conducted with $Fe_2O_3/Al_2O_3/TiO_2$ in the ADMBR were higher than those with Fe_2O_3/Al_2O_3.

The fabricated $Fe_2O_3/Al_2O_3/TiO_2$ oxygen carriers for IPA combustion operated in the ADMBR were identified. As shown in Fig. 9, Fe_2O_3, Fe_2TiO_5 and Al_2O_3 were the major crystalline phases of fresh $Fe_2O_3/Al_2O_3/TiO_2$, and the crystalline phases of reduced oxygen carriers were mostly Fe_3O_4, Al_2FeO_4, Al_2O_3 and TiO_2. Hence, the rhombohedral-structured Fe_2O_3 and the orthorhombic-structured Fe_2TiO_5 were completely reduced to the cubic-structured Fe_3O_4 and Al_2FeO_4,

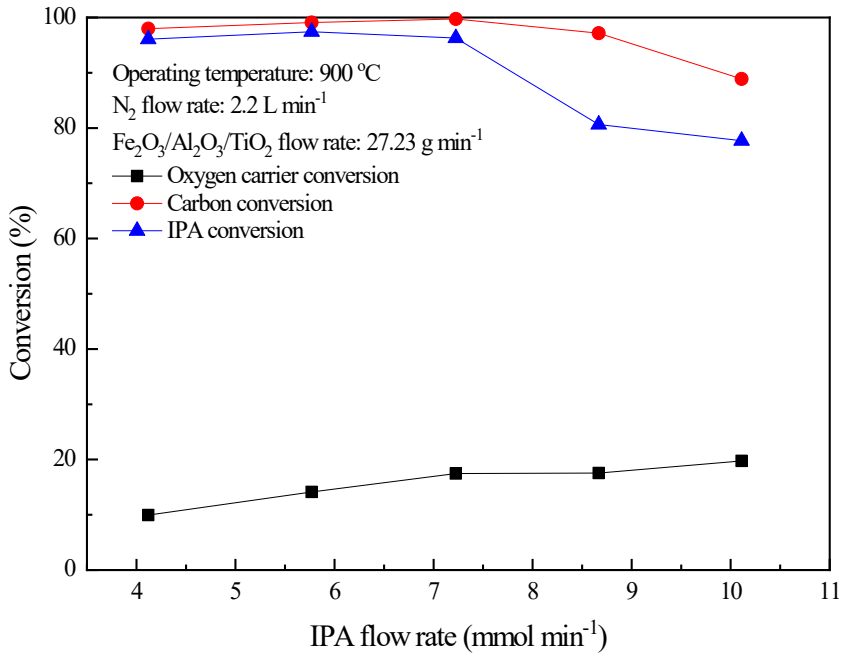

Fig. 8. Effect of IPA flow rate on fuel and oxygen carrier conversions for IPA combustion with $Fe_2O_3/Al_2O_3/TiO_2$ in the ADMBR.

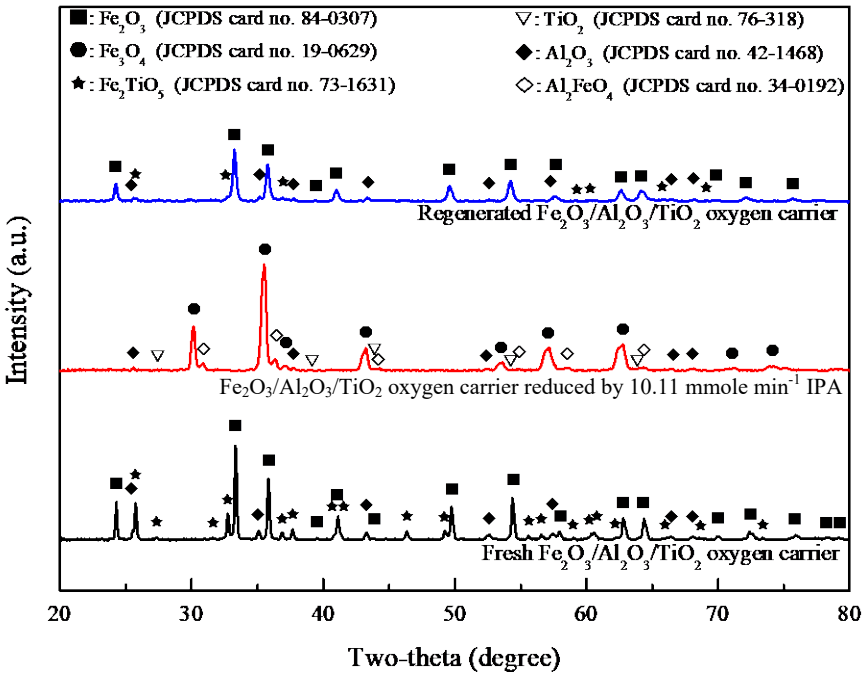

Fig. 9. X-ray diffraction patterns of fresh, reduced and regenerated $Fe_2O_3/Al_2O_3/TiO_2$ for IPA combustion.

comparable observations was previous reported by previous researchers (Abad *et al.*, 2011; Zhu *et al.*, 2016). For regenerated oxygen carriers, Fe_2O_3, Fe_2TiO_5 and Al_2O_3 were observed in the XRD pattern, demonstrating that the reduced oxygen carriers were completely oxidized.

3.4 Kinetic Parameter Determination for the Reduction of Fabricated Oxygen Carriers by Hydrogen

Because hydrogen is the major combustible gas generated by IPA decomposition at temperature above 800°C, the reduction of ferric-oxide oxygen carriers by hydrogen is described by the following simplified reaction (Fan, 2010):

$$H_2 + \frac{1}{3}Fe_2O_3 \leftrightarrow \frac{2}{3}Fe + H_2O \tag{10}$$

Based on the mass balances of oxygen and hydrogen, the conversion of oxygen carriers is determined as:

$$X_{red} = \frac{\int F_{H_2O}\,dt}{\left(\frac{x_{Fe_2O_3} \cdot m_{OC}}{M_{Fe_2O_3}}\right)} \tag{11}$$

$$F_{H_2O} = F_{H_2,in} - F_{H_2} \tag{12}$$

where $F_{H_2,in}$ is the inlet mole flow rate (in mmole min^{-1}) of H_2; F_{H_2} and F_{H_2O} are the outlet molar flow rates (in mmole min^{-1}) of H_2 and H_2O, respectively; m_{OC} is the weight (g) of the fabricated oxygen carriers packed in the reactor; $x_{Fe_2O_3}$ is the fraction of Fe_2O_3 contained in the oxygen carriers; $M_{Fe_2O_3}$ is 159.69 g $mole^{-1}$ as the molecular weight of Fe_2O_3.

The reduction of fabricated Fe_2O_3/Al_2O_3 and $Fe_2O_3/Al_2O_3/TiO_2$ by feeding H_2/N_2 gas mixtures containing 5 to 20 vol.% H_2 was examined in the fixed-bed reactor operated at 875, 900 and 925°C. As shown in Fig. 10, the calculated reduction conversions for experiments conducted with

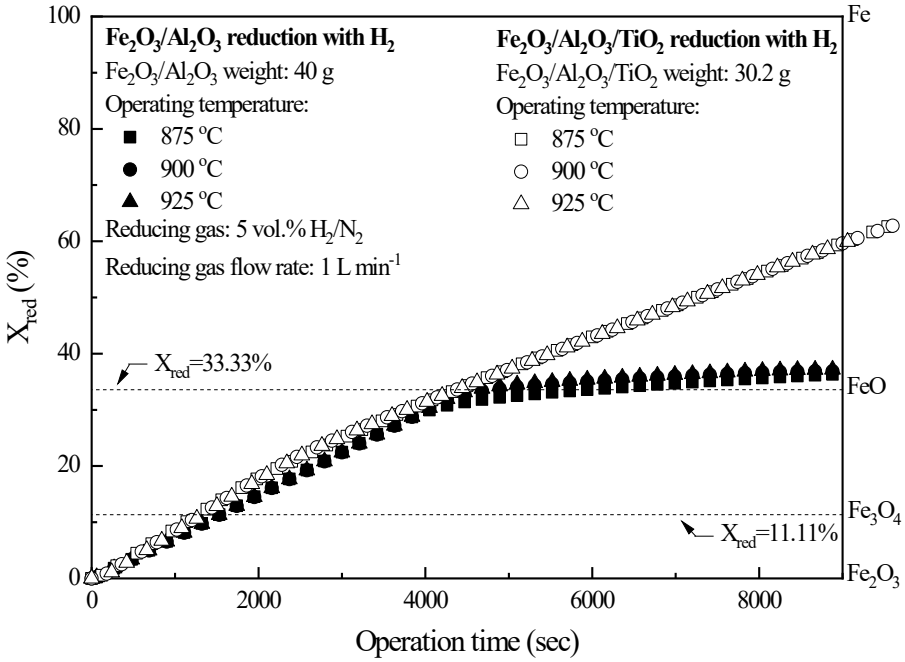

Fig. 10. Effect of operating temperature on the reduction of fabricated iron-based oxygen carriers by hydrogen in the fixed-bed reactor.

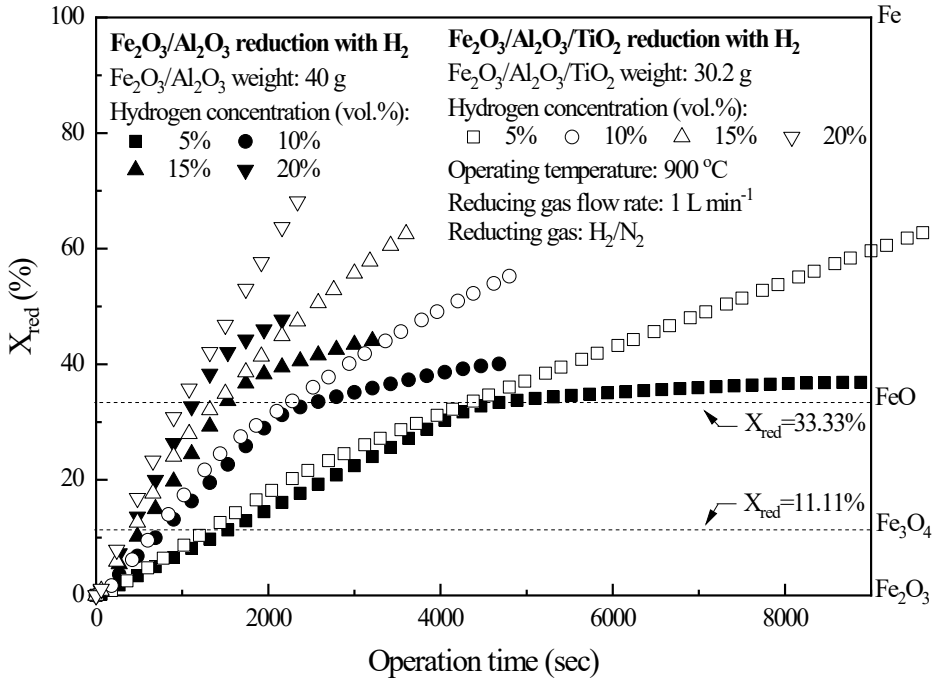

Fig. 11. Effect of inlet hydrogen concentration on the reduction of fabricated iron-based oxygen carriers in the fixed-bed reactor.

$Fe_2O_3/Al_2O_3/TiO_2$ were evidently higher than those with Fe_2O_3/Al_2O_3 after 4,500 second of operation time. For experiments conducted after the Fe_2O_3/Al_2O_3 conversion was observed to be maintained at about 33.33% after 4,500 seconds. The reduction of fabricated oxygen carriers by hydrogen were barely influenced by operating temperature, similar to the observations reported by previous researchers (de Diego *et al.*, 2014; Abad *et al.*, 2015). Fig. 11 exhibits the effect of inlet hydrogen concentrations on the chemical looping combustion of H_2 by fabricated oxygen carriers. The conversions of Fe_2O_3/Al_2O_3 and $Fe_2O_3/Al_2O_3/TiO_2$ reduction were increased for experiments conducted with higher inlet hydrogen concentrations, as described by Reaction (10).

The kinetics for the reduction Fe_2O_3/Al_2O_3 and $Fe_2O_3/Al_2O_3/TiO_2$ by hydrogen were calculated with the shrinking core model (SCM), exercised by most researchers for the application of various oxygen carriers for chemical looping (Abad *et al.*, 2007; Cabello *et al.*, 2014; Abad *et al.*, 2015; Wu and Ku, 2018; Wu and Ku, 2019), as described in Eqs. (13) to (18):

$$1-X_{red}=\left(\frac{r}{R}\right)^3 \tag{13}$$

$$t=\tau_{gf}X_{red}+\tau_{pl}\left[1-3\left(1-X_{red}\right)^{\frac{2}{3}}+2\left(1-X_{red}\right)\right] \tag{14}$$

$$\tau_{gf}=\frac{1000\cdot x_{Fe_2O_3}\cdot\rho_P\cdot R}{3\cdot b\cdot C_{Ag}\cdot M_{Fe_2O_3}\cdot k_g} \tag{15}$$

$$\tau_{pl}=\frac{1000\cdot x_{Fe_2O_3}\cdot\rho_P\cdot R^2}{6\cdot b\cdot C_{Ag}\cdot M_{Fe_2O_3}\cdot D_e} \tag{16}$$

$$D_e=D_{pl,0}\cdot e^{-\frac{Ea_{pl}}{R_gT}-k_dX_{red}} \tag{17}$$

$$k_d = k_{d,0} \cdot e^{-\frac{Ea_d}{R_g T}} \quad (18)$$

where R and r are the radius (m) of the fresh particle and the unreacted core; τ_{gf} and τ_{pl} are the time required for complete conversion of the oxygen carrier when the reaction is controlled by the gas-film diffusion and the product-layer diffusion, respectively. The product-layer (Fe_3O_4, Al_2FeO_4, $FeTiO_3$, FeO, or Fe) generated on the surface of the reduced Fe_2O_3/Al_2O_3 and $Fe_2O_3/Al_2O_3/TiO_2$ is a barrier for the diffusion of fuel molecules and significantly decelerated the reaction rate, especially when high reduction conversions were achieved. C_{Ag} is the inlet molar concentration (mole m^{-3}) of the gaseous fuel; b is the stoichiometric coefficient of gaseous fuel combusted with Fe_2O_3, which is determined to be 1/3 by Reaction (10); k_g is the mass transfer coefficient (m s^{-1}) between gaseous fuel and oxygen carriers; D_e is the effective diffusion diffusivity (m^2 s^{-1}) of gaseous fuel in the product layer; $D_{pl,0}$ (m^2 s^{-1}) and Ea_{pl} (kJ mol^{-1}) are the pre-exponential factor and activation energy for the product-layer diffusion, respectively; k_d, $k_{d,0}$ and Ea_d (kJ mol^{-1}) are the decay constant, pre-exponential factor and activation energy for the product-layer diffusivity, respectively; R_g is the ideal gas constant; T (K) is the operating temperature.

The kinetic parameters for the reduction of prepared iron-based oxygen carriers by hydrogen were summarized in Table 3. The mass transfer coefficients (k_g) for the reduction of Fe_2O_3/Al_2O_3 and $Fe_2O_3/Al_2O_3/TiO_2$ were calculated to be 0.22 and 0.24 mm s^{-1}, respectively; demonstrating that hydrogen molecules can more easily diffuse through the product-layer on Fe_2O_3/Al_2O_3. The higher reduction conversions obtained for experiments conducted with $Fe_2O_3/Al_2O_3/TiO_2$ than those with Fe_2O_3/Al_2O_3 indicates that Fe_2O_3/Al_2O_3 is primarily reduced to FeO, while the $Fe_2O_3/Al_2O_3/TiO_2$ can be further reduced to FeO and Fe. The crystal structure of Fe is denser than that of FeO, and is probably more difficult for hydrogen molecules to pass through the product-layer generated on $Fe_2O_3/Al_2O_3/TiO_2$. Therefore, the mechanism for the overall reduction reaction of Fe_2O_3/Al_2O_3 and $Fe_2O_3/Al_2O_3/TiO_2$ oxygen carriers with H_2 are proposed as Eqs. (19) to (22) based on the experimental results of this study.

For $Fe_2O_3/Al_2O_3/TiO_2$ reduction:

$$Fe_2O_3 + 2Al_2O_3 + H_2 \leftrightarrow 2Al_2FeO_4 + H_2O \quad (19)$$

$$3Fe_2O_3 + H_2 \leftrightarrow 2Fe_3O_4 + H_2O \quad (20)$$

$$Fe_2TiO_5 + TiO_2 + H_2 \leftrightarrow 2FeTiO_3 + H_2O \quad (21)$$

$$FeTiO_3 + H_2 \leftrightarrow Fe + TiO_2 + H_2O \quad (22)$$

4 CONCLUSIONS

Hydrogen is the major combustible gases generated during IPA decomposition at above 800°C. Approximately, more than 95% IPA was combusted for most experiments conducted in the moving-bed reactor with fabricated Fe_2O_3/Al_2O_3 and $Fe_2O_3/Al_2O_3/TiO_2$ operated at inlet IPA flow rate ranged from 4.1 to 5.8 mmol min^{-1} and 4.1 to 7.2 mmol min^{-1}, respectively; in addition, the oxygen carrier conversions were respectively reached less than about 16.3% and 17.5%. Carbon deposition during IPA combustion using $Fe_2O_3/Al_2O_3/TiO_2$ as an oxygen carrier was noticeably avoided. According to the XRD characterization, the cubic structure of Fe_3O_4 and Al_2FeO_4 are the

Table 3. Kinetics parameters for the reduction of fabricated iron-based oxygen carriers by H_2.

Parameter	Symbol	Unit	Fe_2O_3/Al_2O_3	$Fe_2O_3/Al_2O_3/TiO_2$
Mass transfer coefficient	k_g	mm s^{-1}	0.22	0.24
Pre-exponential factor for the product layer diffusion	$D_{pl,0}$	mm^2 s^{-1}	4.79×10^{23}	3.20
Activation energy for the product layer diffusion	Ea_{pl}	kJ mol^{-1}	450.28	37.32
Pre-exponential factor for the product layer diffusivity	$k_{d,0}$	-	501.80	6.50×10^8
Activation energy for the product layer diffusivity	Ea_d	kJ mol^{-1}	26.25	214.09

major crystalline phases generated during the chemical looping combustion of IPA with Fe_2O_3/Al_2O_3. For experiments conducted with $Fe_2O_3/Al_2O_3/TiO_2$, Fe_3O_4, Al_2FeO_4, Al_2O_3, and TiO_2 were identified by the XRD pattern, demonstrating Al_2FeO_4 generated might serve as support materials as well as oxygen carriers during chemical looping combustion. According to the shrinking core model, the mass transfer coefficients (k_g) of Fe_2O_3/Al_2O_3 and $Fe_2O_3/Al_2O_3/TiO_2$ reduction with H_2 were found to be 0.22 and 0.24 mm s^{-1}, while the activation energy for the product layer diffusion reaction (E_{pl}) estimated were about 450 and 37 kJ/mole, respectively. It was noticed that the effective diffusion diffusivity (D_e) of Fe_2O_3/Al_2O_3 oxygen carriers was more easily depended on the oxygen carrier conversion, due to high decay constant (k_d) was obtained for experiments with Fe_2O_3/Al_2O_3 than those with $Fe_2O_3/Al_2O_3/TiO_2$. Therefore, the reduction of fabricated $Fe_2O_3/Al_2O_3/TiO_2$ by hydrogen was observed to further progress to FeO and Fe, and the conversion was obviously higher than that of Fe_2O_3/Al_2O_3, which was primarily reduced to FeO. Hydrogen molecules are found to diffuse more easily through the FeO product-layer on Fe_2O_3/Al_2O_3 than the FeO/Fe product-layer on $Fe_2O_3/Al_2O_3/TiO_2$. However, both Fe_2O_3/Al_2O_3 and $Fe_2O_3/Al_2O_3/TiO_2$ reductions were markedly enhanced with increasing inlet hydrogen concentration and were not obviously influenced by operating temperatures.

ACKNOWLEDGMENTS

This research was supported by Grant MOST 106-3113-E-007-002- from the National Science and Technology Program-Energy, Taiwan, and by Grant MOST 105-2622-E-011-019-CC2 and MOST 103-2221-E-011-002-MY3 from the Ministry of Science and Technology, Taiwan. The authors appreciated China Steel Corp. for providing hematite powders for the preparation of oxygen carriers.

REFERENCES

Abad, A., Adánez, J., García-Labiano, F., de Diego, L.F., Gayán, P., Celaya, J. (2007). Mapping of the range of operational conditions for Cu-, Fe-, and Ni-based oxygen carriers in chemical-looping combustion. Chem. Eng. Sci. 65, 533–549. https://doi.org/10.1016/j.ces.2006.09.019

Abad, A., Adánez, J., Cuadrat, A., García-Labiano, F., Gayán, P., de Diego, L.F. (2011). Kinetics of redox reactions of ilmenite for chemical-looping combustion. Chem. Eng. Sci. 66, 689–702. https://doi.org/10.1016/j.ces.2010.11.010

Abad, A., García-Labiano, F., Gayán, P., de Diego, L.F., Adánez, J. (2015). Redox kinetics of $CaMg_{0.1}Ti_{0.125}Mn_{0.775}O_{2.9-\delta}$ for chemical looping combustion (CLC) and chemical looping with oxygen uncoupling (CLOU). Chem. Eng. J. 269, 67–81. https://doi.org/10.1016/j.cej.2015.01.033

Cabello, A., Abad, A., García-Labiano, F., Gayán, P., de Diego, L.F., Adánez, J. (2014). Kinetic determination of a highly reactive impregnated Fe_2O_3/Al_2O_3 oxygen carrier for use in gas-fueled chemical looping combustion. Chem. Eng. J. 258, 265–280. https://doi.org/10.1016/j.cej.2014.07.083

Chiu, P.C., Ku, Y., Wu, H.C., Kuo, Y.L., Tseng, Y.H. (2014a). Spent isopropanol solution as possible liquid fuel for moving-bed reactor in chemical looping combustion. Energy Fuels 28, 657–665. https://doi.org/10.1021/ef4012438

Chiu, P.C., Ku, Y., Wu, Y.L., Wu, H.C., Kuo, Y.L., Tseng, Y.H. (2014b). Characterization and evaluation of fabricated Fe_2O_3/Al_2O_3 oxygen carriers for chemical looping process. Aerosol Air Qual. Res. 14, 981–990. https://doi.org/10.4209/aaqr.2013.04.0135

Cho, P., Mattisson, T., Lyngfelt, A. (2005). Carbon formation on nickel and iron oxide-containing oxygen carriers for chemical-looping combustion. Ind. Eng. Chem. Res. 44, 668–676. https://doi.org/10.1021/ie049420d

de Diego, L.F., Abad, A., Cabello, A., Gayán, P., García-Labiano, F., Adánez, J. (2014). Reduction and oxidation kinetics of a $CaMn_{0.9}Mg_{0.1}O_{3-\delta}$ oxygen carrier for chemical-looping combustion. Ind. Eng. Chem. Res. 53, 87–103. https://doi.org/10.1021/ie4015765

Fan, L.S. (2010). Chemical looping systems for fossil energy conversions, John Wiley & Sons, Inc., New York, USA.

Fan, L.S., Zeng, L., Luo, S. (2015). Chemical-looping technology platform. AIChE J. 61, 2–22. https://doi.org/10.1002/aic.14695

Giannakeas, N., Lea-Langton, A., Dupont, V., Twigg, M.V. (2012). Hydrogen from scrap tyre oil via steam reforming and chemical looping in a packed bed reactor. Appl. Catal., B 126, 249–257. https://doi.org/10.1016/j.apcatb.2012.07.010

Ishida, M., Takeshita, K., Suzuki, K., Ohba, T. (2005). Application of Fe_2O_3-Al_2O_3 composite particles as solid looping material of the chemical-loop combustor. Energy Fuels 19, 2514–2518. https://doi.org/10.1021/ef0500944

Ku, Y., Wang, L.C., Ma, C.M. (2007). Photocatalytic oxidation of isopropanol in aqueous solution using perovskite-structured $La_2Ti_2O_7$. Chem. Eng. Technol. 30, 895–900. https://doi.org/10.1002/ceat.200700071

Ku, Y., Wu, H.C., Chiu, P.C., Tseng, Y.H., Kuo, Y.L. (2014). Methane combustion by moving-bed fuel reactor with Fe_2O_3/Al_2O_3 oxygen carriers. Appl. Energy 113, 1909–1915. https://doi.org/10.1016/j.apenergy.2013.06.014

Lea-Langton, A., Giannakeas, N., Rickett, G., Dupont, V., Twigg, M.V. (2010). Waste lubricating oil as a source of hydrogen fuel using chemical looping steam reforming. SAE Int. J. Fuels Lubr. 3, 810–818. https://doi.org/10.4271/2010-01-2192

Luo, S., Bayham, S., Zeng, L., McGiveron, O., Chung, E., Majumder, A., Fan, L.S. (2014). Conversion of metallurgical coke and coal using a coal direct chemical looping (CDCL) moving-bed reactor. Appl. Energy 118, 300–308. https://doi.org/10.1016/j.apenergy.2013.11.068

Pimenidou, P., Rickett, G., Dupont, V., Twigg, M.V. (2010). Chemical looping reforming of waste cooking oil in packed bed reactor. Bioresour. Technol. 101, 6389–6397. https://doi.org/10.1016/j.biortech.2010.03.053

Serrano, A., García-Labiano, F., de Diego, L.F., Gayán, P., Abad, A., Adánez, J. (2017). Chemical looping combustion of liquid fossil fuels in a 1 kWth unit using a Fe-based oxygen carrier. Fuel Process. Technol. 160, 47–54. https://doi.org/10.1016/j.fuproc.2017.02.015

Wu, H.C., Ku, Y. (2016). Chemical looping gasification of charcoal with iron-based oxygen carriers in an annular dual-tube moving-bed reactor. Aerosol Air Qual. Res. 16, 1093–1103. https://doi.org/10.4209/aaqr.2015.05.0298

Wu, H.C., Ku, Y. (2018). Enhanced performance of chemical looping combustion of methane with $Fe_2O_3/Al_2O_3/TiO_2$ oxygen carrier. RSC Adv. 8, 39902–39912. https://doi.org/10.1039/C8RA07863G

Wu, H.C., Ku, Y. (2019). Evaluation of iron-based oxygen carrier supported on alumina/ titania for charcoal combustion through chemical looping process. Aerosol Air Qual. Res. 19, 1920–1936. https://doi.org/10.4209/aaqr.2018.06.0222

Zeng, L., Tong, A., Kathe, M., Bayham, S., Fan, L.S. (2015). Iron oxide looping for natural gas conversion in a countercurrent moving-bed reactor. Appl. Energy 157, 338–347. https://doi.org/10.1016/j.apenergy.2015.06.029

Zhu, W., Winterstein, J., Maimon, I., Yin, Q., Yuan, L., Kolmogorov, A.N., Sharma, R., Zhou, G. (2016). Atomic structural evolution during the reduction of α-Fe_2O_3 nanowires. J. Phys. Chem. C 120, 14854–14862. https://doi.org/10.1021/acs.jpcc.6b02033